Co metal nanoparticles deposition inside or outside multi-walled carbon nanotubes via facile support pretreatment

Mariya Kazakova, Andrey Andreev, Alexander Selyutin, Arcady Ishchenko, Alexander Shuvaev, Vladimir A. Kuznetsov, Olga Lapina, Jean-Baptiste d'Espinose de Lacaillerie

Accepted Manuscript

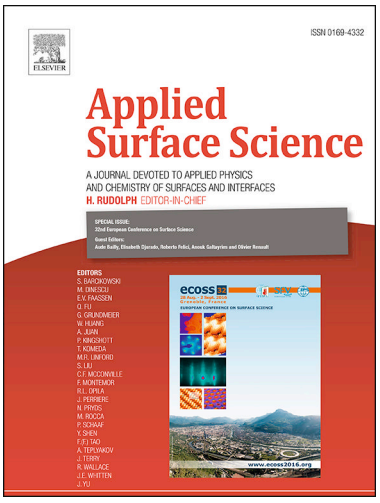

Full Length Article

Co metal nanoparticles deposition inside or outside multi-walled carbon nanotubes via facile support pretreatment

Mariya A. Kazakova, Andrey S. Andreev, Alexander G. Selyutin, Arcady V. Ishchenko, Alexander V. Shuvaev, Vladimir L. Kuznetsov, Olga B. Lapina, Jean-Baptiste d'Espinose de Lacaillerie

PII: S0169-4332(18)31691-X
DOI: https://doi.org/10.1016/j.apsusc.2018.06.124
Reference: APSUSC 39632

To appear in: *Applied Surface Science*

Received Date: 26 March 2018
Revised Date: 26 May 2018
Accepted Date: 13 June 2018

Please cite this article as: M.A. Kazakova, A.S. Andreev, A.G. Selyutin, A.V. Ishchenko, A.V. Shuvaev, V.L. Kuznetsov, O.B. Lapina, J-B. d'Espinose de Lacaillerie, Co metal nanoparticles deposition inside or outside multi-walled carbon nanotubes via facile support pretreatment, *Applied Surface Science* (2018), doi: https://doi.org/10.1016/j.apsusc.2018.06.124

Co metal nanoparticles deposition inside or outside multi-walled carbon nanotubes via facile support pretreatment

*Mariya A. Kazakova** [a, b], *Andrey S. Andreev* [b, c], *Alexander G. Selyutin* [a], *Arcady V. Ishchenko* [a, b], *Alexander V. Shuvaev* [d], *Vladimir L. Kuznetsov* [a, b], *Olga B. Lapina* [a, b], *Jean-Baptiste d'Espinose de Lacaillerie* [c]

[a] Novosibirsk State University, Pirogova 2, Novosibirsk, 630090, Russia

[b] Boreskov Institute of Catalysis, SB RAS, Lavrentieva 5, Novosibirsk 630090, Russia

[c] Soft Matter Science and Engineering (SIMM), UMR CNRS 7615, PSL Research University, ESPCI Paris, 75005, Paris, France

[d] Siberian Transport University, D. Kovalchuk 191, Novosibirsk, 630049, Russia

Abstract

Decoration of one-dimensional multi-walled carbon nanotubes (MWCNTs) with zero-dimensional Co nanoparticles leads to hybrid structures with chemical and electromagnetic features that are not available to the individual components. This work addresses the influence of the nature and structure of MWCNTs on the localization of Co nanoparticles. Depending on synthesis conditions, Co can be deposited on the external or in inner surfaces of the nanotubes. Co/MWCNTs hybrids have been characterized by *in situ* X-ray powder diffraction, high-resolution transmission electron microscopy and ^{59}Co internal field nuclear magnetic resonance. It has been shown that the average diameter (7.2, 9.4 and 18.6 nm), number of walls (5-7, 12-15, 15-20), and functional composition of the MWCNTs have a remarkable effect on the size of Co nanoparticles and their distribution in the structure of MWCNTs. The observed phenomenon has

been rationalized in terms of nanotubes surface properties. Parent MWCNTs being hydrophobic and having limited porosity do not stabilize Co nanoparticles and, therefore, they are localized on the outside surface with relatively large average size and broad size distribution. On the other hand, the oxidation of the MWCNTs resulted in the penetration of Co nanoparticles inside of the nanotubes, presumably because of pore opening as well as increased hydrophilicity of the nanotubes.

Keywords: Co/MWCNT hybrids; metal-support interaction; ferromagnetism; ^{59}Co NMR; HRTEM; *in-situ* XRD

* Corresponding author. E-mail: mas@catalysis.ru (Mariya A. Kazakova)

1. Introduction

The decoration of multi-walled carbon nanotubes (MWCNTs) by cobalt nanoparticles expands the range of their functional properties by providing them with new magnetic, catalytic, electronic and electro-magnetic characteristics. MWCNTs filled with magnetic Co-containing nanoparticles have been proved to be useful for multiple innovations in nanotechnology [1-3], Li/air batteries [4-8], magnetic-storage devices [9], magnetic composites for drug delivery [10, 11], catalysts for different processes [12-18], as well as absorption and microwave irradiation shielding material [19-30]. It is generally accepted that the magnetic properties of nanoparticles are determined by many factors, such as chemical composition [20, 31-35], crystallinity [36, 37], size [37-41] and shape [35, 42-45]. The possible interaction of the nanoparticles with the surrounding matrix and neighboring nanoparticles [46-50] should be also mentioned in the list.

Hence, changing the size, shape, composition and structure of nanoparticles, it is possible, within certain limits, to control the magnetic characteristics of the composite materials. Moreover, intimate interphase contacts between the Co nanoparticles and MWCNTs result in additional synergistic effects. It is thus possible to further tune the electrophysical properties by adjusting, on the one hand, the dielectric component via the MWCNTs structure and content and, on the other hand, the magnetic properties by means of Co nanoparticles loading. This multiplicity of possible leverage makes MWCNTs promising building blocks for the formation of new hybrid materials with new electromagnetic properties. However, this requires a good control of the location and distribution of Co nanoparticles in the structure of MWCNTs.

Depending on the MWCNTs structure parameters (the average size of outer and inner diameters, number of layers, surface area, aspect ratio, defectiveness and the functional composition of their surface) as well as the preparation method of Co/MWCNT hybrids, the size, shape and location of the Co nanoparticles can be varied. Presently, it is still a great challenge to uniformly deposit 3d group magnetic nanoparticles onto both the inner and outer surfaces of MWCNTs without altering its hollow tubular structure. A common synthetic route to produce Co/MWCNT hybrids is incipient wetness impregnation with cobalt salt solutions. However, the specific features of the cobalt nanoparticles formed by this method in, or on, MWCNTs remain unclear. It is very important to consider various factors that may influence the formation and distribution of cobalt particles in the structure of MWCNTs. Such factors include (i) processes occurring in the impregnating solution; (ii) surface charge of MWCNTs; (iii) structure and functional composition of MWCNTs. According to the literature data [51, 52], structure, surface area, surface functional composition, defects of outer layers, size distribution, agglomeration state, and purity of the samples have considerable influence on the surface charge and the reactivity of

carbon nanotubes. MWCNTs are amphoteric by nature, which means that acid and basic functionalities coexist on their surface and that in an aqueous medium. Consequently, depending on the pH and the nature of the MWCNTs surface functionalities, positive or negative charges may be present. In particular, oxidation of pristine MWCNTs leads to the formation of different oxygen-containing groups in the boundary layers, namely carbonyl, carboxyl, lactone, quinone, ether, and hydroxyl groups, the content and distribution of which depend on the oxidation conditions [53, 54]. The appearance of oxygen containing groups can lead under appropriate conditions to the formation of negative charges on the MWCNTs surface, and consequently to a better adsorption of metal cations and, eventually, to a satisfactory dispersion of nanoparticles in the MWCNT structure [54-56].

Previously [22], we investigated the effect of varying Co content nanoparticles, distributed in the structure of MWCNT, on their magnetic and electromagnetic properties. The present work addresses the issue of Co dispersion when synthesizing Co/MWCNT hybrid materials. A special attention has been paid to the impact of the structure and surface functionalities of MWCNTs on the mechanism of metallic cobalt nanoparticles fixation as well as on their ultimate location and size distribution. The structure and morphology of pure and Co-containing MWCNTs has been monitored by high-resolution transmission electron microscope (HRTEM) while the structure of the cobalt metal in the hybrids after the reduction has been essentially investigated by ^{59}Co internal field nuclear magnetic resonance (IF-NMR). This technique provides information about the structure (fcc and hcp stackings) and the average size of Co metal nanoparticles through their magnetically single- and multidomain character. It has been complemented by *in situ* synchrotron X-ray diffraction (XRD) to provide the evolution of all crystalline phases versus temperatures and monitor the evolution of their average sizes.

2. Material and methods

2.1. Synthesis of MWCNTs and functionalization

MWCNTs were synthesized by ethylene decomposition over bimetallic Fe-Co catalysts at 680 °C. The narrowest MWCNTs (labelled MWCNT-7) with an average outer diameter of 7.2 nm and the smaller number of walls (5–7) considered in this study were formed over the 30 wt.% Fe_2Co/Al_2O_3 catalyst; MWCNT with medium outer diameter 9.4 nm and wall number (12–15) over the 40 wt.% Fe_2Co/Al_2O_3 catalysts (labelled MWCNT-9); and the larger diameter MWCNT (labelled MWCNT-18) of 18.6 nm with 15–20 walls over the 40 wt.%$Fe_2Co/CaCO_3$ catalysts [57-60] (see **Figure 1**). These characteristics were established *a posteriori* by statistical analysis of HRTEM images (see below for details of image acquisition methods). The main characteristics of MWCNT-7, MWCNT-9 and MWCNT-18 are presented in the **Table S1**. Removal of the catalyst was carried out by boiling of MWCNT in a 15 % solution of hydrochloric acid for 4 h with vigorous stirring. After acid treatment the precipitate of MWCNT was filtered and washed with distilled water to neutral pH. The BET specific surface areas were determined after this treatment by Nitrogen adsorption using an ASAP-2400 Micromeritics instrument.

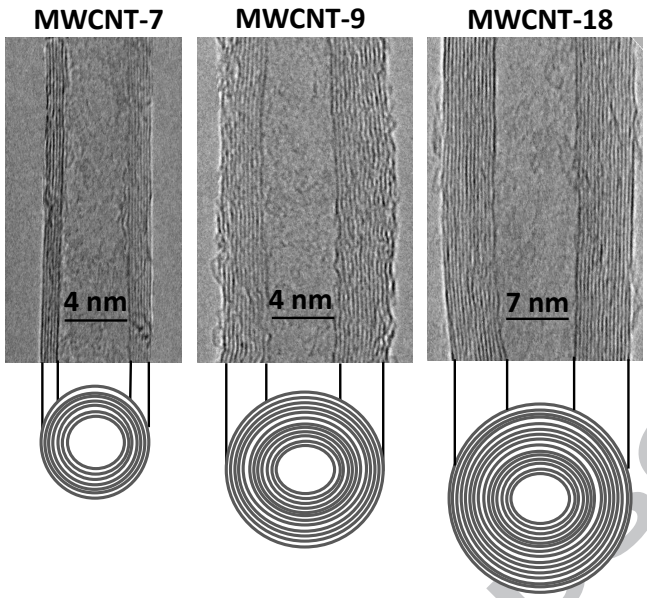

Figure 1. HRTEM images of MWCNT-7, MWCNT-9 and MWCNT-18.

For the investigation of the influence of pre-treatment conditions on the Co particles formation, the oxidation of MWCNT was performed by refluxing of 1 - 2 g MWCNT in concentrated nitric acid for 2 and 8 h. The consequence of this treatment has been evaluated by thermal analysis in a previous publication [61]. Titrimetric analysis of acidic oxygen-containing groups on the MWCNT surface was performed using a reverse acid–base titration technique described by Boehm [62].

2.2. Point of zero charge (PZC) measurements

Surface acid–base properties of the pristine and functionalized MWCNTs at the solid–liquid interface were estimated by determining the PZC according to the standard drift test method (equilibrium pH at high loading) [63-66]. 1 g of each MWCNT samples was placed in 20 ml of aqueous solutions with different initial values of pH (1-13). Then the obtained suspension was stirred on a magnetic stirrer for 1 h at 250 rpm. The pH values were measured until the

equilibrium was established. Therewith, the PZC corresponded to a plateau in the plot of final (equilibrium) pH versus the initial pH. Solutions with the initial pH value ranging from 1 to 13 were prepared with HCl and NaOH. The accuracy of pH measurements was ± 0.15 pH units.

2.3. Co/MWCNT hybrids preparation

Co-containing samples were prepared by incipient wetness impregnation of different types of MWCNTs (7, 9 or 18) with aqua solutions of cobalt nitrate ($Co(NO_3)_2 \cdot 6H_2O$, 98%, Sigma-Aldrich) [22, 67]. After impregnation for 2 h, the sample precursors were dried in air at room temperature during 12 h and then at 110 °C for 6 h followed by calcination at 350 °C for 4 h under an argon atmosphere. They were then reduced in a stream of pure hydrogen (40 ml / min) at 350 °C for 3 h with a heating rate of 2 °C/min. Adjusting the concentration of the cobalt nitrate solutions, samples of about 7.5% Co loading (in weight) were obtained. The exact Co loading was determined by X-ray fluorescence (XRF) using a sequential spectrometer ARL Perform'X with a Rh anode X-ray tube. The element content was assessed using the UniQuant program for standard-less analysis. Prior to analysis, the samples were ground in an agate mortar, and then mixed with cellulose in a ratio of 1 : 5 (wt) in order to obtain the required volume for filling the sample holder.

The prepared samples were denoted as x% Co/MWCNT-(7,9 and 18) Ox or Ox 8h, the number x standing for the cobalt load in weight %; the numbers 7, 9 and 18 denote the MWCNTs with different average diameters, Ox and Ox 8h refer to an eventual oxidative treatment for 2 and 8 h, respectively. Reduced samples were transferred into NMR ampules, which were sealed without contact with air immediately after the reduction procedure.

2.4. *In situ* synchrotron X-ray diffraction (*in situ* XRD)

The crystal phase transformations of the cobalt phase during the reduction of impregnated MWCNT precursors were monitored in situ by XRD at the 3 Precision Diffractometry station of the VEPP-3 beamline of the Siberian Center of Synchrotron and Terahertz Radiation in Novosibirsk (Russian Federation). The samples were placed in an XRK 900 X-ray reaction chamber (Anton Paar, Austria). Heating was performed from room temperature to 700 °C at a rate of 10 °C/min under a flow of diluted H_2 (H_2 rate of 150 ml/sec). An intermediate stage at 350 °C for 200 min was observed. The X-ray patterns were recorded in near real time (60 s per frame) with a laboratory-made (Budker Institute of Nuclear Physics) detector with a 2θ range of 33 ° – 65 ° and steps of ~ 0.01 °. The operating wavelength was 0.1731 nm thus permitting to capture the main reflections of Co metal (PDF 15-806), CoO (PDF 48-1719), Co_3O_4 (PDF 42-1467), and C (PDF 43-1104). The X-ray patterns were interpreted using the Bruker Topas full profile analysis program. The contribution of the baseline was eliminated by conducting additional experiments on the original nanotubes. Additional interpretation of the data was carried out using the Fityk program [68].

Rietveld refinement of the full XRD patterns was carried out using pseudo-Voigt functions. The simulation of reduced 7.7% Co/MWCNT-7 Ox, 7.3% Co/MWCNT-9 Ox, and 8.3% Co/MWCNT-18 Ox required using two fitting peaks for Co metal phases due to inhomogeneous line broadening, *i.e.* one narrow and intense peak originating from particles of larger sizes and one broad one of lower intensity originating from particles of smaller sizes (see **Figure S1** as an example).

2.5. High Resolution Transmission Electron Microscopy (HRTEM)

Morphologies of the MWCNT supports and of the Co/MWCNT hybrids were characterized using a JEOL JEM-2010 microscope operating at 200 kV accelerating voltage which allows a nominal resolution of 1.4 Å. Sample specimens for TEM studies were prepared by dispersion of the powder in dimethylformamide in a glove box under Argon [69]. The dimethylformamide suspension was removed from the box and a drop deposited onto a Micro-mesh copper grid and then quickly transferred to the TEM vacuum chamber where it evaporated. The total time of exposure of the dimethylformamide suspension to atmosphere was 20 s. The MWCNT mean diameters and Co particle size distributions were estimated from a statistical count of the nanotubes from several frames taken on different parts of the samples. Co particle size distributions in the Co/MWCNT samples were estimated by using TEM images containing about 300 - 400 Co particles at magnifications of ×50 000 and ×400 000. The particles outside the MWCNTs were of roughly spherical shape thus only one dimension was measured. However, the particles inside were of oblong geometry giving two characteristic sizes. The values reported in the histograms are the highest values of these two dimensions. Therefore, some particles reported with very large sizes of 15 nm can correspond to long Co wires within the MWCNTs internal space (internal diameter of 4 to 7 nm).

2.6. Internal Field ^{59}Co nuclear magnetic resonance (IF-NMR)

All ^{59}Co IF-NMR experiments were carried out using a Bruker Avance NMR console without external magnetic field application, *i.e.* outside of the NMR magnet, and at ambient temperature. A commercial Bruker broadband static low Q NMR probe head was used. The samples were sealed on-line in the glass reactor used for reduction. Thus, during analysis, the samples did not evolve from the state they reached in the reactor, *i.e.* they were characterized in the same state of

reduction and dispersion. The spectra were acquired using the spin-echo Fourier transform point by point method. The pulse train consisted of two identical pulses of 1 μs duration with an interpulse delay of 8 μs. The number of transients varied from 1 k to 8 k. The sequence repetition rate was 33 Hz due to the very short T_1 relaxation time of ferromagnetic cobalt. Low pulse powers were implemented (less than 10 W delivered at the radio-frequency coil) due to the high enhancement factor of metallic Co [70]. All Gaussian peak positions were determined from the ‘‘optimal’’ spectra in agreement with previous literature results. Only line widths and line intensities were varied, the peak positions remaining fixed during the spectral decompositions. Small manual deviations from the fixed line positions within 0.2 MHz were allowed to optimize the fit. The details of decomposition procedure can be found elsewhere. The quantification of IF-NMR spectra was carried out from this decomposition with correction for the enhancement factor. The detailed explanation of this procedure can be found elsewhere [70].

3. Results

3.1. Effect of the MWCNT structure on the Co particles formation

Multi-walled carbon nanotubes are amphoteric by nature, which means that acidic and basic functionalities coexist on their surface. In an aqueous medium, these functionalities, depending on the pH, provoke a distribution of charges. At pH below the point of zero charge, the balance of charges is positive while for pH above, it is negative. Consequently, electrostatic interaction favors the adsorption of anions in aqueous solutions of pH below the PZC and the one of cations at pH above the PZC. In the case of MWCNTs, the surface chemistry can be modified by oxidative treatment to tune the PZC and favor the adsorption of required ions [71].

The PZC was measured by the pH drift test (**Figure 2**) for the three carbon nanotube types under consideration (MWCNT-7, MWCNT-9 and MWCNT-18, see **Table S1**) before and after

oxidation treatment. Measurements on the three pristine MWCNT samples showed that the PZC pH increased slightly from MWCNT-7 (PZC pH = 6.8) to MWCNT-9 (PZC pH = 7.3) and to MWCNT-18 (PZC pH = 7.9). Considering that the surface charge is driven by (de)protonation, this suggested that increasing wall thickness of pristine MWCNT increased the basicity of the MWCNT external surface. The obtained results are in a good agreement with the literature data stating that the PZC pH of as-produced carbon nanotubes to vary in the range of 5 - 8 pH units [72].

The samples oxidized for 2 h in concentrated nitric acid displayed a drop of PZC pH values down to 3.4, 3.5 and 3.6, respectively for MWCNT-7, -9 and -18 Ox (see also **Figure 2**). Increasing the oxidation treatment time of MWCNT-9 from 2 to 8 h led only to an insignificant augmentation of the measured PZC pH from 3.5 to 3.7 stating that all relevant structural and surface modifications of MWCNTs occurred within the first 2 h of acidic oxidation treatment. Generally, the presence of oxygen containing groups after the oxidation treatment promotes a shift of the PZC pH to a value of about 3 [73-75], that is in agreement with the presented results.

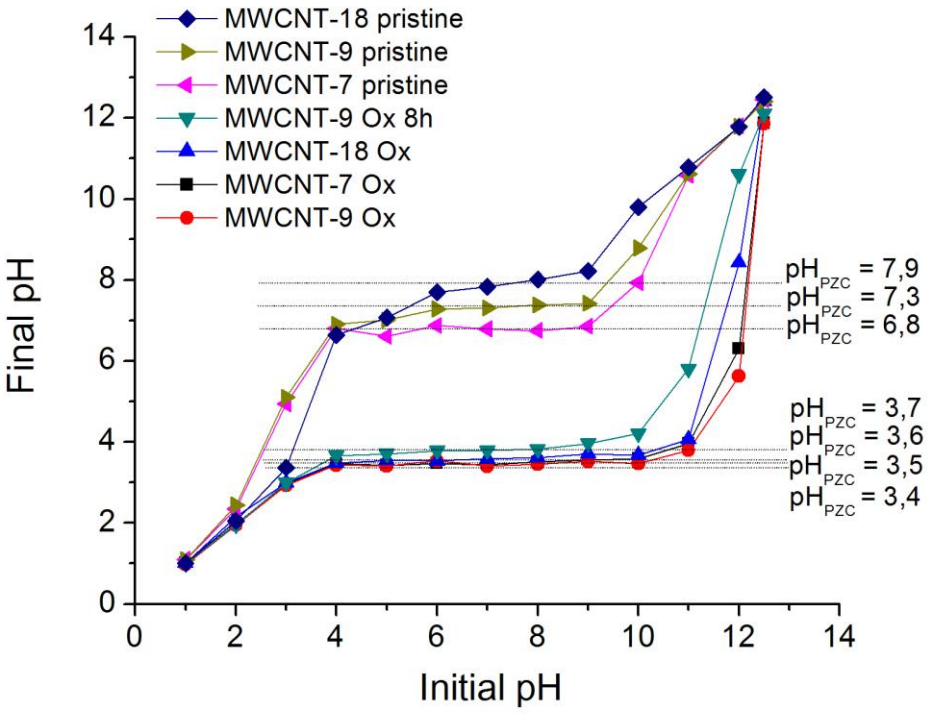

Figure 2. Measurements of PZC by the pH drift method for the three pristine MWCNTs (7, 9 and 18) – upper curves; oxidized for 2 hours (Ox) MWCNTs (7,9 and 18), and after long oxidation treatment for 8 hours (MWCNT-9 Ox 8h) – bottom curves. The value of the plateau of the final pH versus initial pH is equal to the PZC of the given MWCNT. Concentrated nitric acid treatment for 2 h introduced carboxylic functional group on the surface resulting in a drop of the PZC values from 6.8 - 7.9 down to 3.4 -3.6 pH units for all three MWCNTs. Increasing the oxidation treatment time of the MWCNT-9 sample from 2 to 8 h led only to a slight augmentation of the PZC from 3.5 to 3.7 pH units meaning that all relevant structural and surface modifications of the MWCNTs occurred within the first 2 h of acidic oxidation.

Considering that the dramatic shift of the PZC with acidic oxidation was related to the formation of carboxylic functional group on the surface, the density of acidic groups of the

functionalized MWCNTs-(7, 9 and 18) was determined by acid-base titration (**see Table 1**). Using this method, the content of COOH groups in pristine MWCNT was measured to be 0.2 units per 1 nm^{-2}. The surface chemistry of oxidized MWCNTs (7, 9 and 18) and the amount of oxygen-containing groups has already been quantitatively determined by XPS and DTA and published elsewhere [61].

Table 1. Specific surface area, surface density of carboxylic groups and total pore volume of MWCNTs after oxidative treatment for 2 hours

Sample	Average outer diameter of MWCNT, nm	Content of COOH groups per 1 nm^{-2}	S_{BET} (m^2/g)	Total pore volume (mL/g)
MWCNT-7 Ox	7.2	2.7	360	2.48
MWCNT-9 Ox	9.4	2.4	300	2.75
MWCNT-18 Ox	18.6	2.1	130	2.91

3.2. Characterization of Co/MWCNTs hybrids by HRTEM

It has been shown recently [22] that the size and location of cobalt in Co/MWCNT Ox samples depends strongly on the Co loading. Samples with Co concentration up to 10 wt.% mainly contain Co particles within the channels of MWCNTs. As the Co loading increases, the inside population remains constant, but the size distribution of the outside population increases, widens, and shifts toward higher values up to 20-30 nm at 14.5 wt.% loading. Therefore, to isolate the influence of the MWCNT chemistry nature on the structure of Co/MWCNT hybrids, the samples under consideration all exhibited similar Co content, 7.1 - 8.3 wt.%, as determined by XRF.

HRTEM images of reduced Co/MWCNTs hybrids are presented in Figure 3. This figure includes different types of MWCNTs as a support, *i.e.* pristine MWCNT-9 (A), 2 h oxidation small diameter MWCNT-7 Ox (B), oxidized medium diameter MWCNT-9 Ox (C), oxidized large diameter MWCNT-18 (D), and 8 h treated medium diameter MWCNT-9 (E).

The acid–base properties of MWCNTs are of high importance in the Co nanoparticle anchoring. The electrostatic interaction between the MWCNT support and the metal cations in solution depends on the relative values of the solution pH and the MWCNT PZC. The pH of cobalt nitrate aqueous solutions used in this work varied within the range of 4 to 5. At low solution pH values (pH < 3), the speciation of cobalt is Co^{2+} and the MWCNT surface being positively charged, electrostatic repulsion hinders cobalt adsorption. As the pH increases, the MWCNT surface deprotonates and the metal ions adsorbs electrostatically. These phenomena are enhanced since the replacement of protons by metal ions self-propagates the deprotonation process. Simultaneously, the hydrolysis of Co^{2+} at a high pH should be accounted as well. According to the literature in ref. [76-79], cobalt (II) is mainly present as Co^{2+} at pH 8, but at pH 10 it is primarily present as $Co(OH)^{+}$. Consequently, pristine MWCNTs (7, 9 and 18) impregnated with $Co(NO_3)_2$ solution of pH around 4 - 5, that is below their PZC, cannot exhibit cationic adsorption. This led to the observation on the 7.5% Co/MWCNT-9 (**Figure 3A**) of large 20 nm metal Co nanoparticles widely distributed in sizes originating from the reduction of Co oxide precipitated outside of the nanotubes during drying. No Co nanoparticles was observed inside the tubes or decorating their surfaces. Oppositely, the oxidized MWCNTs samples having PZC values lower than the impregnating solution pH, their impregnation under the same conditions resulted in Co^{2+} cationic adsorption. Consequently, two resulting Co nanoparticles populations could be distinguished in the HRTEM images (**Figures 3B-D**). There was a

relatively wide population (σ = 4.5 nm) of sizes centered at 14 nm decorating the outside surface, however, most of the Co nanoparticles were formed mainly inside the MWCNT channels. The internal nanotube surface provokes a restriction of the lateral size to 3 - 5 nm and resulted in the formation of oblong Co particles. Nevertheless, Co particles could still extent further in the longitudinal direction. This phenomenon was reflected in the histograms by a tail of the distribution as only the larger size, *i.e.* elongation length for bi-dimensional structures, is measured during HRTEM image analysis.

Besides pH and PZC, the nucleation and distribution of Co particles are governed as well by the surface structural MWCNT changes caused by the nitric acid oxidative treatments. As a side effect of importance to the issue of further metal deposition, washing with concentrated nitric acid not only eluted away the amorphous part of the samples but increased the defectiveness of the outer layers of the nanotubes. This, together with the opening of the nanotube ends, was likely to favor access of metal, ions or molecules into the internal channels during impregnation or drying, as reported earlier in [22]. Despite the fact that all oxidized samples under considerations had similar PZC, sample Co/MWCNT-7 Ox, with thinner walls and thus more prone to opening during oxidation, exhibited a ratio of ten between the particles populations located in the inside and the outside of the MWCNTs while the Co/MWCNT-9 Ox and Co/MWCNT-18 Ox samples had a more mixed population with a ratio of only about two. The effect of pore openings was further demonstrated by increasing the nitric acid oxidation time on sample MWCNT-9 (**Figure 3E**). The increase of treatment time from 2 to 8 resulted in an insignificant change of the PZC (from 3.5 to 3.7 for 2 and 8 h, respectively), thus the same sorption mechanism must be taken into a consideration. Nevertheless, the prolonged oxidation caused the formation of a larger number of external defects, which facilitated Co ion penetration

via nanotube walls and the ratio of inner to outer cobalt particles raised to about 10 (**Figure 3E**). Additionally, the average size of the outer particles was drastically reduced to 5 nm.

It thus appeared that the duration of the preliminary oxidation treatment is a simple leverage for controlling the size of particle resulting from incipient wetness impregnation with Co nitrate. It favored anchoring the Co particles on the outer surface and simultaneously opened pores facilitating Co diffusion within the internal MWCNT space.

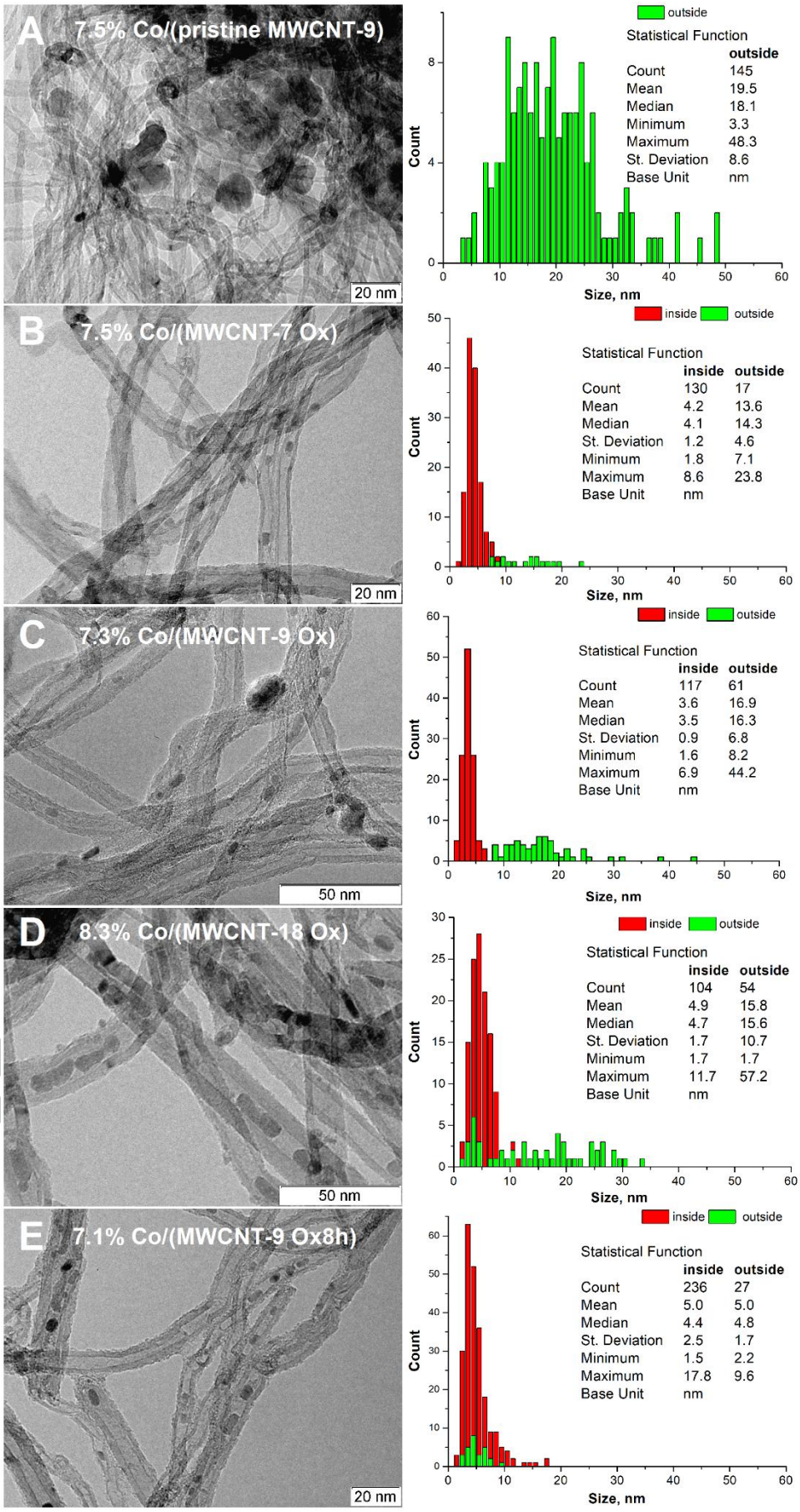
A
7.5% Co/(pristine MWCNT-9)
20 nm
outside
Statistical Function
outside
Count 145
Mean 19.5
Median 18.1
Minimum 3.3
Maximum 48.3
St. Deviation 8.6
Base Unit nm
Count
Size, nm
B
7.5% Co/(MWCNT-7 Ox)
20 nm
inside outside
Statistical Function
inside outside
Count 130 17
Mean 4.2 13.6
Median 4.1 14.3
St. Deviation 1.2 4.6
Minimum 1.8 7.1
Maximum 8.6 23.8
Base Unit nm
Count
Size, nm
C
7.3% Co/(MWCNT-9 Ox)
50 nm
inside outside
Statistical Function
inside outside
Count 117 61
Mean 3.6 16.9
Median 3.5 16.3
St. Deviation 0.9 6.8
Minimum 1.6 8.2
Maximum 6.9 44.2
Base Unit nm
Count
Size, nm
D
8.3% Co/(MWCNT-18 Ox)
50 nm
inside outside
Statistical Function
inside outside
Count 104 54
Mean 4.9 15.8
Median 4.7 15.6
St. Deviation 1.7 10.7
Minimum 1.7 1.7
Maximum 11.7 57.2
Base Unit nm
Count
Size, nm
E
7.1% Co/(MWCNT-9 Ox8h)
20 nm
inside outside
Statistical Function
inside outside
Count 236 27
Mean 5.0 5.0
Median 4.4 4.8
St. Deviation 2.5 1.7
Minimum 1.5 2.2
Maximum 17.8 9.6
Base Unit nm
Count
Size, nm

Figure 3. HRTEM images and particle size histograms of Co/MWCNT hybrids: pristine MWCNT-9 **(A)**, MWCNT-7 Ox **(B)**, MWCNT-9 Ox **(C)**, MWCNT-18 Ox **(D)**, and MWCNT-9 Ox8h **(E)** after the reduction under hydrogen flow. The pristine nanotubes exhibited only large particles on the outer MWCNT surface, whereas 2 h oxidation by nitric acid facilitated Co ion penetration into the internal channel thus resulting in two ensembles of Co nanoparticles: internal and external. Longer acidic treatment leads to the stabilization of smaller Co nanoparticles on the outer MWCNT surface.

3.3 The dynamics of Co nanoparticle formation by *in situ* synchrotron XRD

The dynamics of Co metal particle formation and their sizes have been monitored by *in situ* synchrotron XRD analysis. Note that in these experiments, the heating rate under hydrogen (from room temperature to 350 °C at 10 °.min^{-1}, hold for 200 min, then to 700 °C at 10 °.min^{-1}) differed from the preparation of the samples investigated by HRTEM (from 350 °C to 700 °C at 2°.min^{-1}). The typical time-resolved XRD reduction of the Co/MWCNT-Ox samples exemplified on 8.3% Co/MWCNT-18 Ox sample is displayed in **Figure 4**. As a general observation that is valid for all samples (see **Figure S2**), the phase transition from Co_3O_4 through CoO to Co was induced by temperature increase under hydrogen flow. Co_3O_4 phase diffraction peaks rapidly disappeared from the XRD pattern at temperature above 250 °C. The growth of the CoO (111) diffraction line revealed the initiation of Co reduction, *i.e.* its first stage, from Co_3O_4 to CoO, occurred. This behavior is well documented in the literature [80] but depending on the type of MWCNTs, the temperature behavior of Co_3O_4, CoO and Co crystalline phases leads to various phase transition routes generating different sets of coherent scattering regions (CSR) for the observed phases (see **Figure 5**). It is important to notice that all samples were characterized by a

drastic increase of Co crystallite sizes at temperatures above 550 °C. However, depending on the type of MWCNT-(7, 9 and 18) Ox, the increase in the Co particle size occurred at different rates.

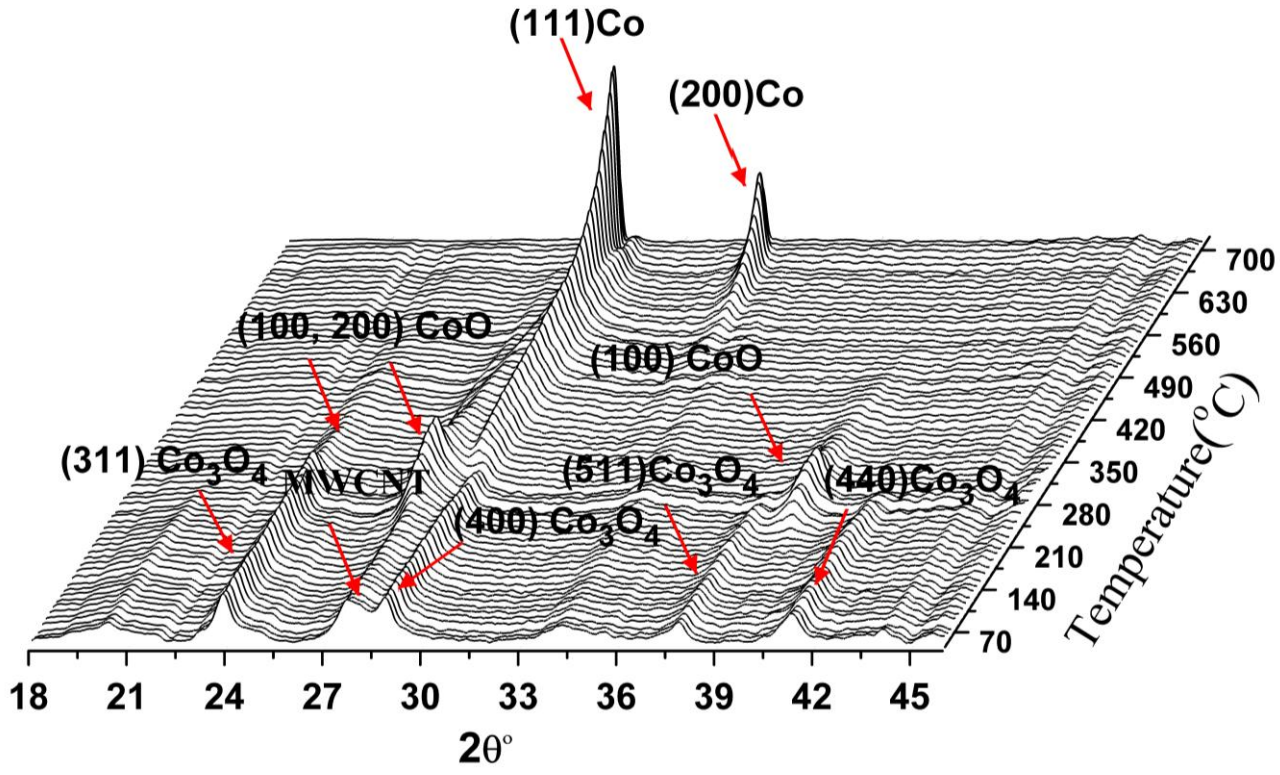

Figure 4. Typical time-resolved XRD patterns of the cobalt phases on MWCNTs-18 Ox (8.3% Co/MWCNT-18 Ox) during reduction under diluted hydrogen (the temperature is ramped). Co fcc metal (PDF 15-806), CoO (PDF 48-1719), Co_3O_4 (PDF 42-1467), and C (PDF 43-1104) indexation are shown. The successive reduction steps of the cobalt spinel into cobalt metal were evidenced but only particles of CSR above 5 nm were visible by XRD. Reduction, complete after the 350 °C stage, was followed by particle sintering up to 700 °C. This process as revealed by the increase of the coherent domain size occurred above 550 °C.

The CSR of all oxide phases of sample 7.7% Co/MWCNT-7 Ox had only a weak dependence on temperature (**Figure 5A**). The Co_3O_4 phase was detected up to the 200 - 300 °C range whereas the CoO phase was observed in the 200 - 520 °C temperature range with a constant CSR value of about 5 to 10 nm. The reduction of Co monoxides to metallic Co began at 290 °C, and, following the temperature increase up to 700 °C, led to a Co metal CSR growth from a few nanometers to between 35 nm and 80 nm depending on the sample. As mentioned in the experimental part, Co metal diffractions have been simulated using two fitting functions reflecting the coexistence of two ensembles of particles inside and outside the MWCNTs.

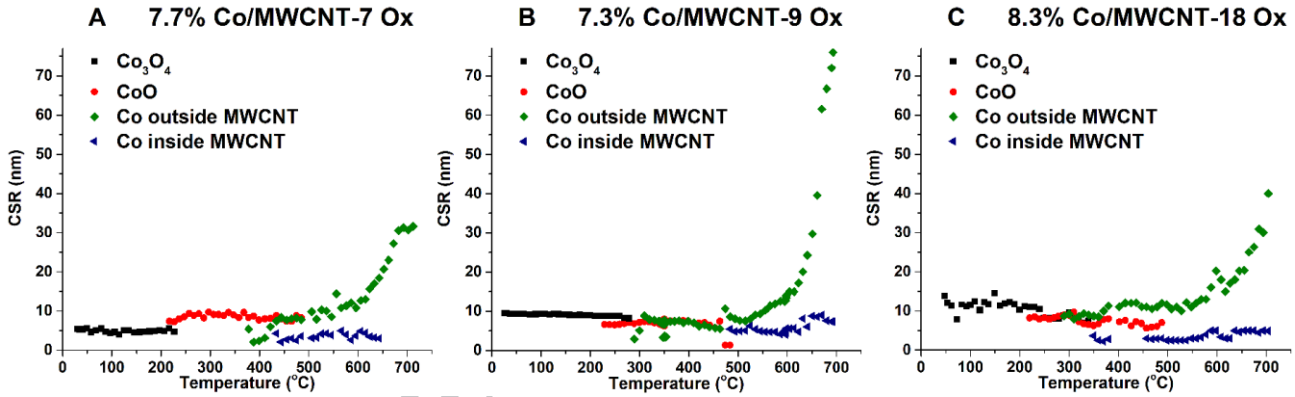

Figure 5. Coherence size domains change with treatment temperature for the observed phases in samples A - 7.7% Co/MWCNT-7 Ox; B - 7.3% Co/MWCNT-9 Ox and C - 8.3% Co/MWCNT-18 Ox.

The CSR values of the Co metal phases versus temperature are displayed in **Figure 5.** A common observation of all samples is the co-existence of two ensembles of Co metal nanoparticles with different sizes, which apparently corresponded to Co particles inside and outside the MWCNTs. The average diameters of the Co crystallites at 700 °C for the Co/MWCNT-7 Ox samples was ~ 4 nm and ~ 35 nm; for Co/MWCNT-9-Ox ~ 4 nm and ~ 80 nm; and for Co/MWCNT-18 Ox ~ 4 nm and ~ 40 nm inside and outside the nanotubes,

respectively. Therefore, as expected, Co metal nanoparticle encapsulation in the internal channels of CNTs promoted, by geometrically constraining the metal, a remarkable size stability versus temperature up to 700 °C. Despite the different thermal history of the samples, the CSR determined in-situ by XRD fully supported the ex-situ HRTEM observation.

3.4. Particles sizes, shapes and structures by IF-NMR

The internal field ^{59}Co NMR (IF-NMR) method is a powerful tool for selective characterization of both structural and magnetic properties of Co metal nanoparticles. It differentiates the structure of Co metal, such as face-centered cubic (fcc) and hexagonal close packed (hcp) Co. Moreover, a magnetic information can be extracted as well as magnetically multi- and single-domain particles give rise to different spectral lines.

The IF-NMR spectra of Co obtained on different diameter MWCNTs are displayed in **Figure 6.** The spectra distinguished five unresolved different lines arising from different cobalt stackings. The maximum of all samples corresponded to fcc cobalt in single-domain particles (~ 216.5 MHz). The resonance of cobalt in multidomain fcc particles was shifted by about 3 MHz to lower frequencies due to the cancellation of the demagnetization field. The higher frequency lines were attributed to the hcp cobalt (~ 219 MHz, ~ 221.5 MHz and 224 MHz) [81, 82]. The observation of the three lines due to hcp Co magnetic anisotropy was a peculiarity of Co supported on MWCNTs. In previous studies of Co metal particles supported on other supports like alumina [83], SiC [81], or others [84] only one broad line is observed.

Co/MNCNT-7 Ox and Co/MWCNT-9 Ox showed an increase of the hcp cobalt relative contribution with the increase of total cobalt amount in the sample. This could be associated with increasing Co particle size according to ref. [85] stating a preferential stabilization of fcc cobalt in smaller nanoparticles. Therefore, the hcp ratio relative growth could be a side effect of the

average particle size increase (**Table 2**). Another observation that could be related to the increasing average Co particle size with MWCNT diameter change was the shift of the fcc single-domain resonance from 216 to 217 MHz. This additional high frequency shift of a single-domain line position is an indication of increasing demagnetization field associated with particle growth (see ref. [86]).

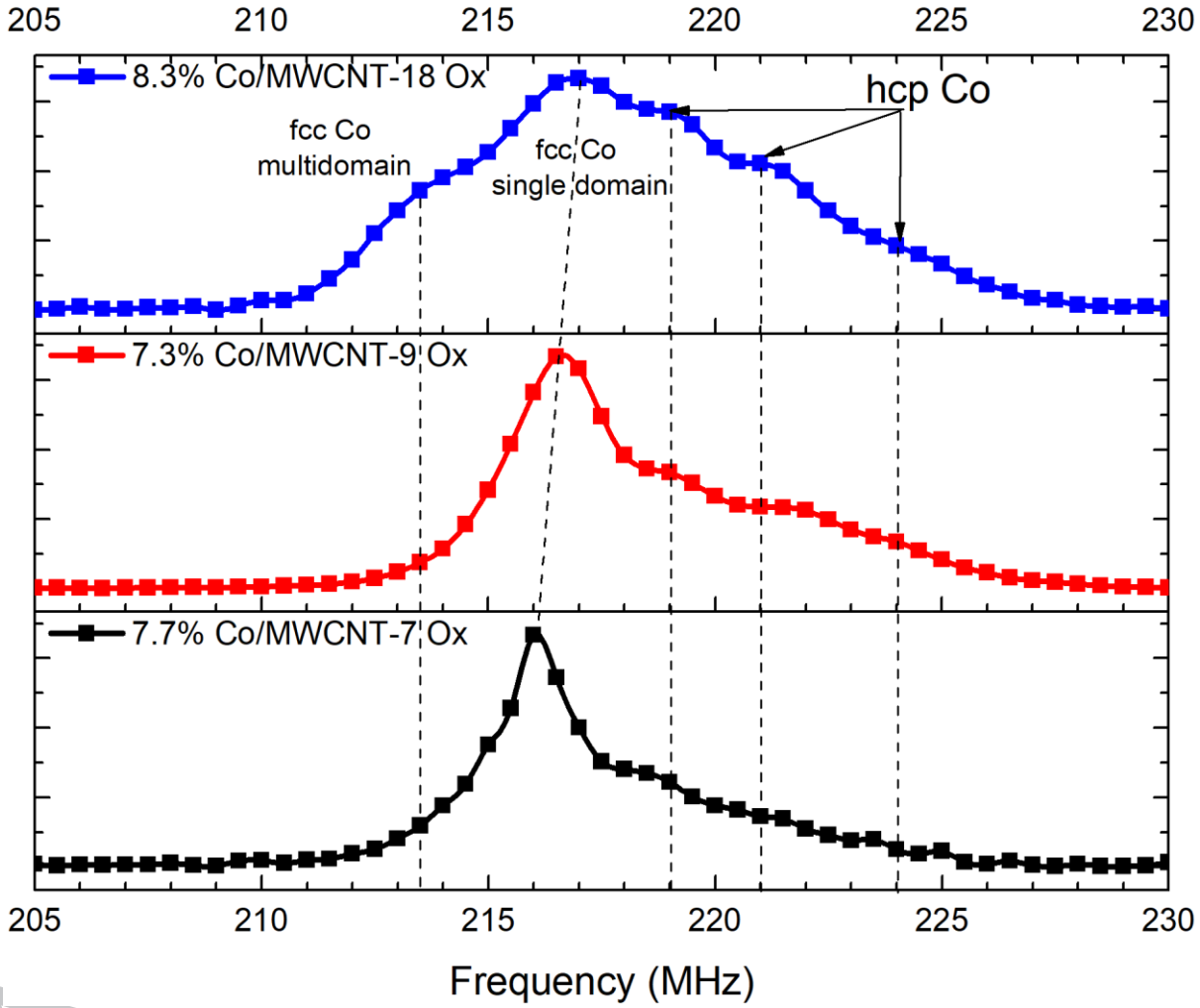

Figure 6. Optimal ^{59}Co IF-NMR spectra of Co/MWCNT-7 Ox (bottom, black), Co/MWCNT-9 Ox (middle, red) and Co/MWCNT-18 Ox hybrids (top, blue) after reduction. Observation of a multidomain fcc resonance correlated with the occurrence of large multidomain (more than 50 –

70 nm) particles by HRTEM. The high frequency displacement of single-domain fcc line was a result of the increase of the demagnetization field with the particle average size.

The spectrum of Co/MWCNT-18 Ox (**Figure 6** top) differed from the ones of Co/MWCNT-7 Ox (**Figure 6** bottom) and Co/MWCNT-9 Ox (**Figure 6** middle) due to a new line appearing at ~ 213 MHz, which was a contribution of multidomain fcc cobalt nanoparticles exceeding 50-70 nm in size [87]. Indeed, among the three, it was in the Co/MWCNT-18 Ox sample that the largest outside Co particles were detected by HRTEM. The exact fraction of large particles could be hardly assessed by IF-NMR as the hcp multidomain cobalt resonance, which should appear at 214 MHz, was superimposed with the one of Co in single-domain fcc particles. It was solely possible to determine a minimal fraction of Co atoms in multidomain particles, which was equal to the 213 MHz line fcc multidomain contribution (~ 18 at. %) (see **Table 2**).

Table 2. Decomposition of the ^{59}Co IF-NMR spectra corrected for the enhancement factor (see **Figure S3**) giving the content of each line. The hcp/fcc ratio was recalculated from the fit of IF-NMR spectra. The accuracy of the total fcc (hcp) phase determination was ±5%.

Sample	Multi-domain fcc, at.%	Single-domains fcc, at. %	hcp 219 MHz, at.%	hcp 221 MHz, at.%	hcp 224 MHz, at.%	hcp/fcc
7.7% Co/MWCNT-7 Ox	-	66	19	13	2	0.5
7.3% Co/MWCNT-9 Ox	-	60	24	13	3	0.7
8.3% Co/MWCNT-18 Ox	18	39	19	17	7	0.8

4. Discussion

Many processes, such as hydrolysis, dissociation, and complexation, must be taken into consideration to determine the different ionic forms existing in aqueous solutions. Taking into account the relevant hydrolysis and dissociation constants, it can be predicted that 99.997 % of the Co in the impregnation solution of Co nitrate (II) at pH 3.95 was in the form of Co^{2+} (see confirmatory calculations in the supplementary materials). The value of the PZC of the oxidized MWCNTs was always around of 3.5 for all nanotubes types used in this work. The small difference between the initial pH of the solution and the PZC of the oxidized MWCNTs thus insured that no significant redistribution of the speciation of Co occurred. One could thus safely only consider the existence of solvated Co^{2+} ions, which have 0.208 nm radius [88]. The penetration of Co ions into 4 and 7 nm internal nanotube channels was thus possible.

For the pristine nanotubes (pH_{ZPC} = 7 - 8), the pH of the same initial Co nitrate (II) aqueous solution was buffered towards a value close to the PZC. Consequently, ionic speciation changed but Co^{2+} remained largely dominant (99.43% of all Co in solution). Therefore, an increase of the overall pH of the MWCNT system / aqueous solution of Co nitrate up to 7 did not lead to a significant redistribution of ionic forms and cobalt ions remained essentially in the form of Co^{2+}. There was thus no electrostatic barrier to the adsorption of Co ions on the surface of the pristine MWCNTs. Nevertheless, Co particles were detected solely outside of carbon nanotubes Co according to HRTEM images (**Figure 3**). There are several factors explaining this phenomenon. First, the surface and internal channels of pristine MWCNTs are known to be hydrophobic, leading to Co salt sedimentation during drying followed by nitrate decomposition during

calcination. Second, the internal channels of pristine MWCNTs were closed thus no Co ions could penetrate inside them.

Oppositely, the inner and outer surfaces of oxidized MWCNTs possess a pronounced hydrophilic character [89]. As a consequence, inner and outer surface deposition is favored by wetting while capillary forces promotes the solution ingress within the inner space of the nanotubes. Consequently, after reduction, Co metal nanoparticles were observed both within the nanotubes and on their external surfaces. Moreover, the oxidation treatment contributed to the defectiveness of the carbon nanotube walls (**Figure 3E**), providing both entry points for the ions within the inner space and anchoring sites. This led to the stabilization of smaller Co particle on the surface as oxidation time increases from 2 to 8 h.

To summarize, MWCNTs could be produced and modified to confer them considerably different structure and surface properties. The formation of Co nanoparticles in the internal channels of MWCNTs was mainly tuned by (i) acid-base properties of the MWCNTs; (ii) availability of the internal channels (ends, wall defects) and (iii) higher affinity of the aqueous solution of metal precursor during the impregnation to the inner surface (namely, hydrophilic properties). The inner MWCNT channels filling rate decreased according to the following series: MWCNT-9 Ox 8h > MWCNT-7 Ox > MWCNT-9 Ox > MWCNT-18 Ox > MWCNT (7,9 and 18) pristine.

5. Conclusion

The effect of the MWCNTs nature (diameter and number of walls) as well as their oxidative pretreatment on the Co nanoparticle formation by incipient wetness impregnation followed by reduction has been investigated by *in situ* XRD, HRTEM and ^{59}Co IF-NMR.

Pristine MWCNTs (7, 9 and 18), hydrophobic and with limited porosity, did not stabilize Co nanoparticle which only formed outside of the MWCNTs with an average particles size of 20 nm and a very wide size distribution as well as poor resistance to sintering. Pretreatment by oxidation in nitric acid for 2 h of MWCNTs (7, 9 and 18) leads to the co-existence of Co populations inside and outside the nanotubes with nanoparticle diameters of 5 and 15 nm, respectively. This was due to increased hydrophilicity and adsorption energy as well as pore opening. This pore opening is all the more easier that the wall are thinner. The prolongation of the oxidation time to 8 h resulted in the occurrence of Co nanoparticles mainly inside the nanotubes channels with average diameter 5 nm. The remaining outside Co nanoparticle population saw its average size decrease to 5 nm due to a better anchoring of the Co precursor on the external surfaces. These results, derived from ex-situ HRTEM analysis, were confirmed by ^{59}Co IF-NMR.

As revealed by *in situ* synchrotron XRD, Co nanoparticles located inside the internal channels of MWCNTs retained their original size of 5 nm even after heating up to 700 °C, while Co nanoparticles on the outer surface underwent intensive sintering, which led to particle size increase up to 80 nm.

In conclusion, we have shown that post-synthesis modification of MWCNT structures opens a possibility for controlling the Co nanoparticle preferable location outside, on, or inside the nanotubes depending on the targeted properties. For various applications including catalysts [4, 13, 15, 90, 91], deposition of small particles on the external surface of the nanotubes will be preferred. For magnetic applications, relatively large outside nanomagnets will be desired while the steric size control resulting from a localization in the internal space of the nanotubes will be essential to tune electro-magnetic properties for dielectric or shielding applications [19-22].

Acknowledgements

The reported study was funded by the Russian Foundation for Basic Research via grant 16-32-60046 mol_a_dk (Mariya A. Kazakova). Olga B. Lapina and Andrey S. Andreev are grateful to the Russian Foundation for Basic Research, which provided the ^{59}Co NMR studies via grant 17-53-150018. A. S. Andreev was also supported in part by a PhD grant from the French Embassy in Moscow and by the Société des Amis de l'ESPCI.

Supplementary Material

The additional in situ XRD patterns, ^{59}Co IF-NMR spectra, and the calculation of dissociation are available free of charge in Supplementary Material.

References

[1] Y. Lisunova, J. Heidler, I. Levkivskyi, I. Gaponenko, A. Weber, C. Ch, L.J. Heyderman, M. Kläui, P. Paruch, Optimal ferromagnetically-coated carbon nanotube tips for ultra-high resolution magnetic force microscopy, Nanotechnology, 24 (2013) 105705.

[2] L.O. Ermolaeva, S.N. Gusev, V.E. Skorohodov, V.Y. Petrov, V.M. Sapozhnikov, L.V. Mironov, Magnetic Force Microscopy of Nanostructured Co/Pt Multilayer Films with Perpendicular Magnetization, Materials, 10 (2017) 1034.

[3] H. Kuramochi, T. Uzumaki, M. Yasutake, A. Tanaka, H. Akinaga, H. Yokoyama, A magnetic force microscope using CoFe-coated carbon nanotube probes, Nanotechnology, 16 (2005) 24-27.

[4] T.H. Yoon, Y.J. Park, Carbon nanotube/Co_3O_4 composite for air electrode of lithium-air battery, Nanoscale Res. Lett., 7 (2012) 28.

[5] T. Chen, Z. Zhang, B. Cheng, R. Chen, Y. Hu, L. Ma, G. Zhu, J. Liu, Z. Jin, Self-Templated Formation of Interlaced Carbon Nanotubes Threaded Hollow Co_3S_4 Nanoboxes for High-Rate and Heat-Resistant Lithium–Sulfur Batteries, J. Am. Chem. Soc., 139 (2017) 12710-12715.

[6] K. Olszowska, J. Pang, P.S. Wrobel, L. Zhao, H.Q. Ta, Z. Liu, B. Trzebicka, A. Bachmatiuk, M.H. Rummeli, Three-dimensional nanostructured graphene: Synthesis and energy, environmental and biomedical applications, Synth. Met., 234 (2017) 53-85.

[7] Q. Su, G. Du, J. Zhang, Y. Zhong, B. Xu, Y. Yang, S. Neupane, K. Kadel, W. Li, In Situ Transmission Electron Microscopy Investigation of the Electrochemical Lithiation–Delithiation of Individual Co_9S_8/Co-Filled Carbon Nanotubes, ACS Nano, 7 (2013) 11379-11387.

[8] S. Abouali, A. Garakani, X. Mohammad, Zheng-Long, J.-K. Kim, $NiCo_2O_4$/CNT nanocomposites as bi-functional electrodes for Li ion batteries and supercapacitors, Carbon, 102 (2016) 262-272.

[9] A. Reyhani, S.Z. Mortazavi, S. Mirershadi, A.Z. Moshfegh, P. Parvin, A.N. Golikand, Hydrogen Storage in Decorated Multiwalled Carbon Nanotubes by Ca, Co, Fe, Ni, and Pd Nanoparticles under Ambient Conditions, J. Phys. Chem. C, 115 (2011) 6994-7001.

[10] A. Masotti, A. Caporali, Preparation of Magnetic Carbon Nanotubes (Mag-CNTs) for Biomedical and Biotechnological Applications, Int. J. Mol. Sci., 14 (2013) 24619-24642.

[11] X. Liu, I. Marangon, G. Melinte, C. Wilhelm, C. Ménard-Moyon, B.P. Pichon, E. O., K. Aubertin, B. W., P.-H. C., S. Bégin-Colin, A. Bianco, F. Gazeau, D. Bégin, Design of Covalently Functionalized Carbon Nanotubes Filled with Metal Oxide Nanoparticles for Imaging, Therapy, and Magnetic Manipulation, ACS Nano, 8 (2014) 11290-11304.

[12] S. Bartling, C. Yin, I. Barke, K. Oldenburg, H. Hartmann, V. von Oeynhausen, M.-M. Pohl, K. Houben, E.C. Tyo, S. Seifert, P. Lievens, K.-H. Meiwes-Broer, S. Vajda, Pronounced Size

Dependence in Structure and Morphology of Gas-Phase Produced, Partially Oxidized Cobalt Nanoparticles under Catalytic Reaction Conditions, ACS Nano, 9 (2015) 5984-5998.

[13] H. Zhang, Y.A. Alhamed, W. Chu, Z. Ye, A. AlZahrani, L. Petrov, Controlling Co-support interaction in Co/MWCNTs catalysts and catalytic performance for hydrogen production via NH_3 decomposition, Appl. Catal., A, 464–465 (2013) 156-164.

[14] H. Zhang, Y.A. Alhamed, A. Al-Zahrani, M. Daous, H. Inokawa, Y. Kojima, L.A. Petrov, Tuning catalytic performances of cobalt catalysts for clean hydrogen generation via variation of the type of carbon support and catalyst post-treatment temperature, Int. J. Hydrogen Energy, 39 (2014) 17573-17582.

[15] C.-H. Kuo, W. Li, W. Song, Z. Luo, A.S. Poyraz, Y. Guo, Ma, A.W. K., S.L. Suib, J. He, Facile Synthesis of Co_3O_4@CNT with High Catalytic Activity for CO Oxidation under Moisture-Rich Conditions, ACS Appl. Mater. Interfaces, 6 (2014) 11311-11317.

[16] X. Zhang, Z. Wu, X. Zhang, L. Li, Y. Li, H. Xu, X. Li, X. Yu, Z. Zhang, Y. Liang, H. Wang, Highly selective and active CO_2 reduction electrocatalysts based on cobalt phthalocyanine/carbon nanotube hybrid structures, Nat Commun, 8 (2017) 14675.

[17] J. Yu, Y. Zhong, W. Zhou, Z. Shao, Facile synthesis of nitrogen-doped carbon nanotubes encapsulating nickel cobalt alloys 3D networks for oxygen evolution reaction in an alkaline solution, J. Power Sources, 338 (2017) 26-33.

[18] K. Elumeeva, M.A. Kazakova, D.M. Morales, D. Medina, A. Selyutin, G. Golubtsov, Y. Ivanov, V. Kuznetzov, A. Chuvilin, H. Antoni, M. Muhler, W. Schuhmann, J. Masa, Bifunctional Oxygen Reduction/Oxygen Evolution Activity of Mixed Fe/Co Oxide Nanoparticles with Variable Fe/Co Ratios Supported on Multiwalled Carbon Nanotubes, ChemSusChem, 11 (2018) 1204-1214.

[19] D.-L. Zhao, J.-M. Zhang, X. Li, Z.-M. Shen, Electromagnetic and microwave absorbing properties of Co-filled carbon nanotubes, J. Alloys Compd., 505 (2010) 712-716.

[20] H. Lin, H. Zhu, H. Guo, L. Yu, Microwave-absorbing properties of Co-filled carbon nanotubes, Mater. Res. Bull., 43 (2008) 2697-2702.

[21] J. Sui, C. Zhang, J. Li, Z. Yu, W. Cai, Microwave absorption and catalytic activity of carbon nanotubes decorated with cobalt nanoparticles, Mater. Lett., 75 (2012) 158-160.

[22] A.S. Andreev, M.A. Kazakova, A.V. Ishchenko, A.G. Selyutin, O.B. Lapina, V.L. Kuznetsov, J.-B. d'Espinose de Lacaillerie, Magnetic and dielectric properties of carbon nanotubes with embedded cobalt nanoparticles, Carbon, 114 (2017) 39-49.

[23] F. Wen, F. Zhang, Z. Liu, Investigation on Microwave Absorption Properties for Multiwalled Carbon Nanotubes/Fe/Co/Ni Nanopowders as Lightweight Absorbers, J. Phys. Chem. C, 115 (2011) 14025-14030.

[24] T.A. Saleh, V.K. Gupta, Column with CNT/magnesium oxide composite for lead(II) removal from water, Environ. Sci. Pollut. Res., 19 (2012) 1224-1228.

[25] T.A. Saleh, Simultaneous adsorptive desulfurization of diesel fuel over bimetallic nanoparticles loaded on activated carbon, J. Cleaner Prod., 172 (2018) 2123-2132.

[26] T.A. Saleh, T.D. Shuaib, G.I. Danmaliki, M.A. Al-Daous, Carbon-Based Nanomaterials for Desulfurization: Classification, Preparation, and Evaluation, in: A.S. Tawfik (Ed.) Applying Nanotechnology to the Desulfurization Process in Petroleum Engineering, IGI Global, Hershey, PA, USA, 2016, pp. 154-179.

[27] T.A. Saleh, S.A. Al-Hammadi, Insights into the Fundamentals and Principles of the Oil and Gas Industry: The Impact of Nanotechnology, in: T.A. Saleh (Ed.) Nanotechnology in Oil and

Gas Industries: Principles and Applications, Springer International Publishing, Cham, 2018, pp. 1-35.

[28] K. Wang, J. Pang, L. Li, S. Zhou, Y. Li, T. Zhang, Synthesis of hydrophobic carbon nanotubes/reduced graphene oxide composite films by flash light irradiation, Front. Chem. Sci. Eng., (2018). DOI:10.1007/s11705-018-1705-z

[29] I. Arief, S. Biswas, S. Bose, FeCo-Anchored Reduced Graphene Oxide Framework-Based Soft Composites Containing Carbon Nanotubes as Highly Efficient Microwave Absorbers with Excellent Heat Dissipation Ability, ACS Appl. Mater. Interfaces, 9 (2017) 19202-19214.

[30] M.A. Kazakova, N.V. Semikolenova, E.Y. Korovin, S.I. Moseenkov, A.S. Andreev, A.S. Kachalov, V.L. Kuznetsov, V.I. Suslyev, M.A. Matsko, V.A. Zakharov., *In situ* polymerization technique for obtaining composite materials based on polyethylene, multiwalled carbon nanotubes and cobalt nanoparticles, Russ. J. Appl. Chem., 91 (2018) 126-134.

[31] X.-j. Fan, X. Li, Preparation and magnetic property of multiwalled carbon nanotubes decorated by Fe_3O_4 nanoparticles, New Carbon Mater., 27 (2012) 111-116.

[32] Z. Klencsár, P. Németh, Z. Sándor, T. Horváth, I.E. Sajó, S. Mészáros, J. Mantilla, J.A.H. Coaquira, V.K. Garg, E. Kuzmann, G. Tolnai, Structure and magnetism of Fe–Co alloy nanoparticles, J. Alloys Compd., 674 (2016) 153-161.

[33] A.M. Abdalla, F. Abdel, R. Abdel, S. Ghosh, I.K. Puri, Magnetoresponsive conductive colloidal suspensions with magnetized carbon nanotubes, J. Magn. Magn. Mater., 421 (2017) 292-299.

[34] Y. Cao, Preparation and Magnetic Properties of a Multi-Walled Carbon Nanotube-Iron Oxide Nanoparticle Composite, Fuller. Nanotub. Car. N., 23 (2015) 623-626.

[35] B. Issa, M.I. Obaidat, A.B. Albiss, Y. Haik, Magnetic Nanoparticles: Surface Effects and Properties Related to Biomedicine Applications, Int. J. Mol. Sci., 14 (2013) 21266-21305.

[36] T. Hayashi, S. Hirono, M. Tomita, S. Umemura, Magnetic thin films of cobalt nanocrystals encapsulated in graphite-like carbon, Nature, 381 (1996) 772-774.

[37] Q. Li, C.W. Kartikowati, S. Horie, T. Ogi, T. Iwaki, K. Okuyama, Correlation between particle size/domain structure and magnetic properties of highly crystalline Fe_3O_4 nanoparticles, Sci. Rep., 7 (2017) 9894.

[38] N.S. Gajbhiye, S. Sharma, A.K. Nigam, R.S. Ningthoujam, Tuning of single to multi-domain behavior for monodispersed ferromagnetic cobalt nanoparticles, Chem. Phys. Lett., 466 (2008) 181-185.

[39] J. Lee, S.G. Kwon, J.-G. Park, T. Hyeon, Size Dependence of Metal–Insulator Transition in Stoichiometric Fe_3O_4 Nanocrystals, Nano Lett., 15 (2015) 4337-4342.

[40] S. Upadhyay, K. Parekh, B. Pandey, Influence of crystallite size on the magnetic properties of Fe_3O_4 nanoparticles, J. Alloys Compd., 678 (2016) 478-485.

[41] Y.W. Jun, J.W. Seo, J. Cheon, Nanoscaling laws of magnetic nanoparticles and their applicabilities in biomedical sciences, Acc. Chem. Res., 41 (2008) 179-189.

[42] L. Yonghua, Z. Yaohua, L. Tong, S. Masaaki, L. Xingguo, Synthesis of single crystalline triangular and hexagonal Ni nanosheets with enhanced magnetic properties, Nanotechnology, 17 (2006) 1797–1800.

[43] A.K. Singh, O.N. Srivastava, K. Singh, Shape and Size-Dependent Magnetic Properties of Fe_3O_4 Nanoparticles Synthesized Using Piperidine, Nanoscale Res. Lett., 12 (2017) 298.

[44] N.R. Jana, Y. Chen, X. Peng, Size- and Shape-Controlled Magnetic (Cr, Mn, Fe, Co, Ni) Oxide Nanocrystals via a Simple and General Approach, Chem. Mater., 16 (2004) 3931-3935.

[45] P. Guardia, A. Labarta, X. Batlle, Tuning the Size, the Shape, and the Magnetic Properties of Iron Oxide Nanoparticles, J. Phys. Chem. C, 115 (2011) 390-396.

[46] C.B. Murray, S. Sun, H. Doyle, T. Betley, Monodisperse 3d Transition-Metal (Co,Ni,Fe) Nanoparticles and Their Assembly into Nanoparticle Superlattices, MRS Bulletin, 26 (2012) 985-991.

[47] S. Oyarzún, A. Tamion, F. Tournus, V. Dupuis, M. Hillenkamp, Size effects in the magnetic anisotropy of embedded cobalt nanoparticles: from shape to surface, Sci. Rep., 5 (2015) 14749.

[48] H. Shokrollahi, L. Avazpour, Influence of intrinsic parameters on the particle size of magnetic spinel nanoparticles synthesized by wet chemical methods, Particuology, 26 (2016) 32-39.

[49] M.A. Kazakova, V.L. Kuznetsov, N.V. Semikolenova, S.I. Moseenkov, D.V. Krasnikov, M.A. Matsko, A.V. Ishchenko, V.A. Zakharov, A.I. Romanenko, O.B. Anikeeva, E.N. Tkachev, V.I. Suslyaev, V.A. Zhuravlev, K.V. Dorozkin, Comparative study of multiwalled carbon nanotube/polyethylene composites produced via different techniques, Phys. Status Solidi B, 251 (2014) 2437-2443.

[50] S. Mørup, Hansen, M. Fougt, C. Frandsen, Magnetic interactions between nanoparticles, Beilstein J. Nanotechnol., 1 (2010) 182-190.

[51] C.-W. Chen, M.-H. Lee, Ab initio calculations of dimensional and adsorbate effects on the workfunction of single-walled carbon nanotube, Diamond Relat. Mater., 12 (2003) 565-571.

[52] F.E. Leys, C. Amovilli, I.A. Howard, N.H. March, A. Rubio, Surface charge model of a carbon nanotube: self-consistent field from Thomas–Fermi theory, J. Phys. Chem. Solids, 64 (2003) 1285-1288.

[53] Z. Zhang, L. Pfefferle, G.L. Haller, Characterization of functional groups on oxidized multi-wall carbon nanotubes by potentiometric titration, Catal. Today, 249 (2015) 23-29.

[54] F. Rodríguez-Reinoso, The role of carbon materials in heterogeneous catalysis, Carbon, 36 (1998) 159-175.

[55] G. Ertl, H. Knözinger, J. Weitkamp, Preparation of Solid Catalysts, Wiley, 2008.

[56] C. Prado-Burguete, A. Linares-Solano, F. Rodríguez-Reinoso, C.S.-M. de Lecea, The effect of oxygen surface groups of the support on platinum dispersion in Pt/carbon catalysts, J. Catal., 115 (1989) 98-106.

[57] V.L. Kuznetsov, S.N. Bokova-Sirosh, S.I. Moseenkov, A.V. Ishchenko, D.V. Krasnikov, M.A. Kazakova, A.I. Romanenko, E.N. Tkachev, E.D. Obraztsova, Raman spectra for characterization of defective CVD multi-walled carbon nanotubes, Phys. Status Solidi B, 251 (2014) 2444-2450.

[58] S.N. Bokova-Sirosh, V.L. Kuznetsov, A.I. Romanenko, M.A. Kazakova, D.V. Krasnikov, E.N. Tkachev, Y.I. Yuzyuk, E.D. Obraztsova, Investigation of defectiveness of multiwalled carbon nanotubes produced with Fe–Co catalysts of different composition, J. Nanophoton., 10 (2016) 012526 (012521-012510).

[59] A.S. Andreev, D.V. Krasnikov, V.I. Zaikovskii, S.V. Cherepanova, M.A. Kazakova, O.B. Lapina, V.L. Kuznetsov, J.B. d'Espinose de Lacaillerie, Internal field 59Co NMR study of cobalt-iron nanoparticles during the activation of $CoFe_2$/CaO catalyst for carbon nanotube synthesis, J. Catal., 358 (2018) 62-70.

[60] V.L. Kuznetsov, V.I. Suslyaev, I.O. Dorofeev, M.A. Kazakova, S.I. Moseenkov, T.E. Smirnova, D.V. Krasnikov, Investigation of electromagnetic properties of MWCNT aerogels produced via catalytic ethylene decomposition, Phys. Status Solidi B, 252 (2015) 2519-2523.

[61] I. Mazov, V.L. Kuznetsov, I.A. Simonova, A.I. Stadnichenko, A.V. Ishchenko, A.I. Romanenko, E.N. Tkachev, O.B. Anikeeva, Oxidation behavior of multiwall carbon nanotubes with different diameters and morphology, Appl. Surf. Sci., 258 (2012) 6272-6280.

[62] H.P. Boehm, Some aspects of the surface chemistry of carbon blacks and other carbons, Carbon, 32 (1994) 759-769.

[63] Annual Book of ASTM Standard, in: Standard Test Method for Determination of Contact pH with Activated Carbon, Philadelphia PA ,United State of America, 2011.

[64] X. Hao, L. Quach, J. Korah, W.A. Spieker, J.R. Regalbuto, The control of platinum impregnation by PZC alteration of oxides and carbon, J. Mol. Catal. A: Chem., 219 (2004) 97-107.

[65] R.M. Mironenko, O.B. Belskaya, T.I. Gulyaeva, A.I. Nizovskii, A.V. Kalinkin, V.I. Bukhtiyarov, A.V. Lavrenov, V.A. Likholobov, Effect of the nature of carbon support on the formation of active sites in Pd/C and Ru/C catalysts for hydrogenation of furfural, Catal. Today, 249 (2015) 145-152.

[66] R.M. Mironenko, O.B. Belskaya, V.P. Talsi, T.I. Gulyaeva, M.O. Kazakov, A.I. Nizovskii, A.V. Kalinkin, V.I. Bukhtiyarov, A.V. Lavrenov, V.A. Likholobov, Effect of γ-Al_2O_3 hydrothermal treatment on the formation and properties of platinum sites in Pt/γ-Al_2O_3 catalysts, Appl. Catal., A, 469 (2014) 472-482.

[67] M.A. Shuvaeva, G.S. Litvak, V.A. Varnek, G.A. Bukhtiyarova, Preparation of supported iron-containing catalysts from a $FeSO_4$ solution: The effect of the support, Kinetics and Catalysis, 50 (2009) 874.

[68] M. Wojdyr, Fityk: a general-purpose peak fitting program, J. Appl. Crystallogr., 43 (2010) 1126-1128.

[69] G.M. Mikheev, V.L. Kuznetsov, K.G. Mikheev, T.N. Mogileva, M.A. Shuvaeva, S.I. Moseenkov, Laser modification of optical properties of a carbon nanotube suspension in dimethylformamide, Tech. Phys. Lett., 39 (2013) 337-340.

[70] A.S. Andreev, O.B. Lapina, S.V. Cherepanova, A New Insight into Cobalt Metal Powder Internal Field 59Co NMR Spectra, Appl. Magn. Reson., 45 (2014) 1009-1017.

[71] A.Y. Khodakov, W. Chu, P. Fongarland, Advances in the Development of Novel Cobalt Fischer−Tropsch Catalysts for Synthesis of Long-Chain Hydrocarbons and Clean Fuels, Chem. Rev. (Washington, DC, U. S.), 107 (2007) 1692-1744.

[72] S. Fogden, R. Verdejo, B. Cottam, M. Shaffer, Purification of single walled carbon nanotubes: The problem with oxidation debris, Chem. Phys. Lett., 460 (2008) 162-167.

[73] C. Lu, H. Chiu, Chemical modification of multiwalled carbon nanotubes for sorption of Zn^{2+} from aqueous solution, Chem. Eng. J., 139 (2008) 462-468.

[74] Y. Liu, L. Gao, A study of the electrical properties of carbon nanotube-$NiFe_2O_4$ composites: Effect of the surface treatment of the carbon nanotubes, Carbon, 43 (2005) 47-52.

[75] Perez-Aguilar, N. Veronica, Muñoz-Sandoval, D.-F. Emilio, P. Elizabeth, Rangel-Mendez, J. Rene, Adsorption of cadmium and lead onto oxidized nitrogen-doped multiwall carbon nanotubes in aqueous solution: equilibrium and kinetics, J. Nanopart. Res., 12 (2010) 467-480.

[76] E.T. Gray, Atlas of metal-ligand equilibria in aqueous solution, J. Kragten, Ellis Horwood Limited, Chichester, England, 1978, 781 pp, in: Synth. React. Inorg. Met.-Org. Chem., Taylor & Francis, 1979, pp. 395-397.

[77] C.F. Baes, R.E. Mesmer, The hydrolysis of cations, Wiley, New York, 1976.

[78] M.A. Khan, E. Gee, J. Choi, M. Kumar, W. Jung, T.C. Timmes, H.-C. Kim, B.-H. Jeon, Adsorption of cobalt onto graphite nanocarbon–impregnated alginate beads: equilibrium, kinetics, and thermodynamics studies, Chem. Eng. Commun., 201 (2014) 403-418.

[79] N.V. Plyasunova, Y. Zhang, M. Muhammed, Critical evaluation of thermodynamics of complex formation of metal ions in aqueous solutions. V. hydrolysis and hydroxo-complexes of Co^{2+} at 298.15 K, Hydrometallurgy, 48 (1998) 153-169.

[80] N. Fischer, E. van Steen, M. Claeys, Preparation of supported nano-sized cobalt oxide and fcc cobalt crystallites, Catal. Today, 171 (2011) 174-179.

[81] A.S. Andreev, J.-B. d'Espinose de Lacaillerie, O.B. Lapina, A. Gerashenko, Thermal stability and hcp-fcc allotropic transformation in supported Co metal catalysts probed near operando by ferromagnetic NMR, Phys. Chem. Chem. Phys., 17 (2015) 14598-14604.

[82] V.V. Matveev, D.A. Baranov, G.Y. Yurkov, N.G. Akatiev, I.P. Dotsenko, S.P. Gubin, Cobalt nanoparticles with preferential hcp structure: A confirmation by X-ray diffraction and NMR, Chem. Phys. Lett., 422 (2006) 402-405.

[83] A.S. Andreev, O.B. Lapina, J.B. d'Espinose de Lacaillerie, A.A. Khassin, EFfect of alumina modification on the structure of cobalt-containing Fischer-Tropsch synthesis catalysts according to internal-field 59Co NMR data, J. Struct. Chem., 54 (2013) 102-110.

[84] Y. Liu, J. Luo, Y. Shin, S. Moldovan, O. Ersen, A. Hebraud, G. Schlatter, C. Pham-Huu, C. Meny, Sampling the structure and chemical order in assemblies of ferromagnetic nanoparticles by nuclear magnetic resonance, Nat Commun, 7 (2016) 11532.

[85] O. Kitakami, H. Sato, Y. Shimada, F. Sato, M. Tanaka, Size effect on the crystal phase of cobalt fine particles, Phys. Rev. B, 56 (1997) 13849-13854.

[86] Y.D. Zhang, J.I. Budnick, W.A. Hines, S.A. Majetich, E.M. Kirkpatrick, Microstructure and magnetic behavior of carbon-coated Co nanoparticles studied by nuclear magnetic resonance, Appl. Phys. Lett., 76 (2000) 94-96.

[87] D.L. Leslie-Pelecky, R.D. Rieke, Magnetic Properties of Nanostructured Materials, Chem. Mater., 8 (1996) 1770-1783.

[88] Y. Marcus, Ionic radii in aqueous solutions, Chem. Rev. (Washington, DC, U. S.), 88 (1988) 1475-1498.

[89] O. Ersen, J. Werckmann, M. Houllé, M.-J. Ledoux, C. Pham-Huu, 3D Electron Microscopy Study of Metal Particles Inside Multiwalled Carbon Nanotubes, Nano Lett., 7 (2007) 1898-1907.

[90] S.A. Chernyak, E.V. Suslova, A.V. Egorov, K.I. Maslakov, S.V. Savilov, V.V. Lunin, Effect of Co crystallinity on Co/CNT catalytic activity in CO/CO_2 hydrogenation and CO disproportionation, Appl. Surf. Sci., 372 (2016) 100-107.

[91] T.O. Eschemann, W.S. Lamme, R.L. Manchester, T.E. Parmentier, A. Cognigni, M. Rønning, K.P. de Jong, Effect of support surface treatment on the synthesis, structure, and performance of Co/CNT Fischer–Tropsch catalysts, J. Catal., 328 (2015) 130-138.

Graphical abstract

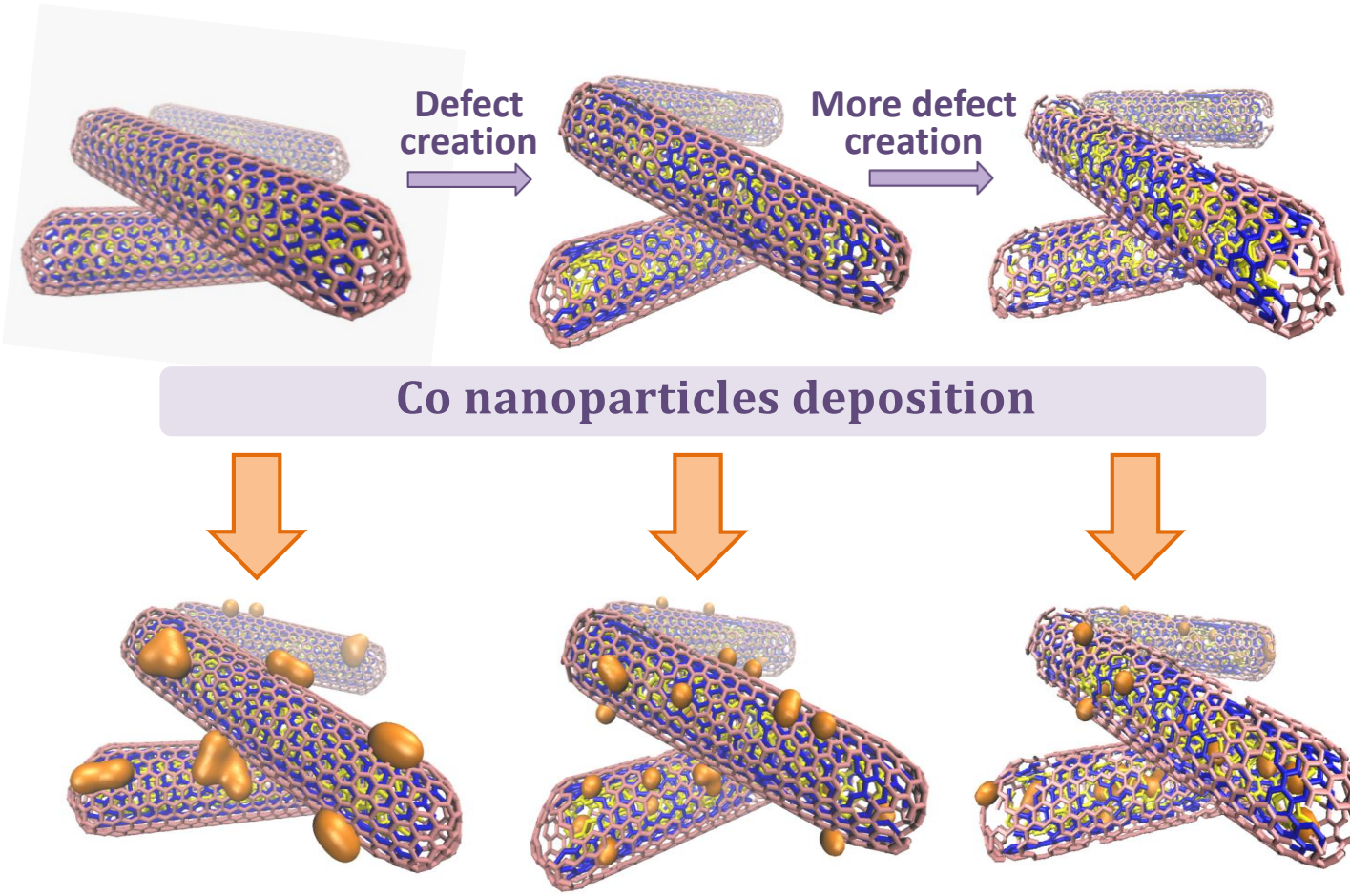

Highlights

- Co/MWCNT hybrids with controllable localization of Co nanoparticles are obtained.
- Localization of Co nanoparticles depends on the nature and structure of MWCNTs.
- Hydrophobic/hydrophilic properties of MWCNT surface strongly affect Co deposition.
- Oxidized MWCNTs with thin walls stabilize Co nanoparticles mainly inside their channels.
- Oxidation of MWCNTs leads to the decrease of Co nanoparticles average size.